C. R. Mecanique 343 (2015) 670–679

Contents lists available at ScienceDirect

Comptes Rendus Mecanique

www.sciencedirect.com

Acoustic metamaterials and phononic crystals

Dynamic reconfiguration of magneto-elastic lattices

Marshall Schaeffer [a,*], Massimo Ruzzene [b]

[a] Daniel Guggenheim School of Aerospace Engineering, Georgia Institute of Technology, 270 Ferst Dr., Atlanta, GA 30332, USA
[b] George W. Woodruff School of Mechanical Engineering, Georgia Institute of Technology, 801 Ferst Dr., Atlanta, GA 30332, USA

ARTICLE INFO

Article history:
Received 3 March 2015
Accepted 22 June 2015
Available online 16 July 2015

Keywords:
Reconfiguration
Transformation dynamics
Magneto-elastic
Phase transition
Multistable

ABSTRACT

The dynamic reconfiguration of two-dimensional (2D) magneto-elastic structures is studied with the goal of enabling the design of reconfigurable architectured materials. Changes in magnetization modify the energy landscape of hexagonal lattices and lead to their reconfiguration as a result of the application of a dynamic input. Such reconfiguration significantly alters the dynamics of the structure and its mechanical properties. Energy landscapes and the dynamics of reconfiguration are analyzed through the detailed study of a unit cell and the description of loci of equilibrium within the energy landscape, as well as numerical simulations on finite lattices undergoing reconfiguration. Results show the occurrence of a transition front propagating within the 2D structures according to a triangular pattern bounded by transition bands that separate different orientation domains within the structure.

1. Introduction

The internal configuration of an architectured structural system is known to have significant effects on its properties, both static [1] and dynamic in the context of waves and vibrations [2,3]. In previous studies by the authors [4], magneto-elastic lattices are shown to be capable of reconfiguring into a variety of different stable configurations, which exhibit different mechanical properties. Changing the properties of structures in this way is of interest for creating novel adaptive structures and devices. Systems that can reconfigure to display regions of different configurations, or to feature different orientations of anisotropic configurations, can be useful for controlling not only the global but also the local properties of a structure, and may find use in applications such as wave steering and focusing. Structures with locally varying properties could also be instrumental in creating waveguides that route waves in paths that are determined by the local configuration, similar to those in [5].

Effective use of structural reconfigurations requires the detailed analysis of the properties of the lattice in its different multi-stable states, along with the characterization of the conditions, parameters and overall process that leads to the desired lattice configuration. Changes in structural properties due to static or quasi-static reconfiguration have been investigated, for example, in [6–10]. However, in order to access a richer set of final configurations and to find paths for faster transitions, dynamic lattice reconfigurations should be considered. The specifics of the dynamic reconfiguration can determine how certain regions of a structure reconfigure, allowing local property control and grading. A fast rate of reconfiguration could be valuable in applications intended for protection from short events and shocks that can damage organs, electronics, or other delicate objects. The reconfiguration of the structure itself can even be a way of absorbing energy

* Corresponding author.
E-mail addresses: mschaeffer3@gatech.edu (M. Schaeffer), ruzzene@gatech.edu (M. Ruzzene).

http://dx.doi.org/10.1016/j.crme.2015.06.007
1631-0721/

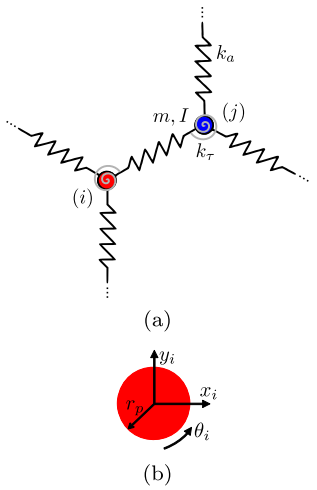

Fig. 1. (Color online.) Schematic of mechanical connectivity between two adjacent particles i and j (a), and particle degrees of freedom (b).

without damaging the protective structure, by redirecting or storing incoming energy within the structure as demonstrated by [11].

One dimensional (1D) systems composed of bistable interactions have received attention in terms of their dynamic reconfiguration, including the study of "transition front" propagation, or the rate at which reconfiguration occurs [12–16]. The energy profile of bistable interactions, i.e. how the interaction potential varies with the distance between interacting entities, provides important insight into the paths leading to configurational changes and the initial and final static topologies. The ability to shape such profiles could be the primary means by which the dynamic reconfiguration of a structure can be designed. Of importance is the identification of energy minima that are associated with equilibrium configurations that correspond to different geometries and the relative energetic contents of such minima to estimate the amount of energy required for the reconfiguration to take place. While the previously mentioned references focus on more general systems, dynamic reconfiguration has also been studied specifically to understand martensitic transformation in shape memory alloys, which includes both 1D [17,18] and 2D [19,20] studies.

In contrast to 1D dynamic reconfiguration investigations, the study of 2D systems is still in need of much attention. In order to realize reconfigurable devices as suggested previously, the understanding of reconfiguration dynamics in higher dimensions is in fact required. Therefore, the focus of this paper is to conduct an initial study of dynamic structural changes in 2D structures, using a magneto-elastic hexagonal honeycomb lattice as an example. The energy profile associated with a unit cell of the lattice is employed as a means to predict the reconfiguration characteristics. However, in 2D systems, additional information is required to investigate the spatial extent of the reconfiguration, which leads to non-periodic topologies characterized by regions of reconfigured cells whose shape and spatial extent is clearly defined by the lattice parameters and by the input energy. These regions are so far investigated and highlighted by the numerical simulations conducted as part of this study, and should be better understood and characterized in future investigations. Unit cell analyses and numerical experiments presented herein are however expected to provide insights for future modeling and design of 2D dynamically reconfigurable structures.

The paper is organized as follows. Following this introduction, a summary of the model of the lattice is provided based on prior work by the authors [4]. Unit cell energy profiles are then investigated to identify potential configurations associated with energy minima. Next, the numerical simulation approach is described, and results of the simulations are presented and discussed. Finally, conclusions and final recommendations are provided.

2. Lattice model description

The magneto-elastic lattices are composed of a periodic layout of magnetized masses connected by axial and torsional elastic springs (Fig. 1(a)).[1] Particles are of mass m, radius r_p, and rotational inertial I. Furthermore, all magnets are characterized by the same magnetization magnitude. Axial and torsional springs all have stiffness k_a and k_τ respectively. Particles motion is described by two translational degrees of freedom and one angle to describe rotation about an axis perpendicular to the plane of the lattice. The generalized coordinates for the i-th particle are therefore $\boldsymbol{q_i} = [x_i, y_i, \theta_i]^T$ (Fig. 1(b)). Particle-to-particle interactions include: (1) magnetic interactions, (2) elastic interactions through axial and torsional springs, and

[1] Reprinted from M. Schaeffer and M. Ruzzene, Wave propagation in multistable magneto-elastic lattices, Int. J. Solids Struct. 56–57 (2015) 78–95, copyright (2015), with permission from Elsevier.

(3) dissipation in the form of viscous damping. The modeling approach is described in detail in [4] so simply a summary is provided below.

2.1. Magnetic interactions

The permanent magnets in the lattices are modeled as magnetically rigid point dipole moments [21]. The motion of the masses remains in the lattice plane and the magnetic dipole moments are perpendicular to the plane of motion. This constraint allows simplification of the force between two dipoles, which is given by [22]:

$$\boldsymbol{f}_{ij}^{(m)} = \frac{3\mu_0}{4\pi}\frac{m_i m_j}{r_{ij}^4}\boldsymbol{n} = \frac{\psi^{(m)}}{r_{ij}^4}\boldsymbol{n} \tag{1}$$

where $\psi^{(m)} = 3\mu_0 m_i m_j/4\pi$, with μ_0 denoting the permeability of free space. Also, m_i and m_j are the dipole moments of particles i and j, $\boldsymbol{r}_{ij}$ is the position of j relative to i, $\boldsymbol{n} = \boldsymbol{r}_{ij}/r_{ij}$ is a unit vector. Since magnetic forces act over an infinite distance, every particle in a finite lattice interacts with every other particle magnetically.

2.2. Elastic interactions

The particles are connected by axial springs of stiffness k_a and torsional springs of stiffness k_τ. A simplified model for contact is applied between particles that are closer together than $r_\mathrm{c} = 2r_\mathrm{p}$, where r_p is the particle radius, and r_0 denotes the unreformed length of the springs. The contact stiffness between two particles is proportional to the stiffness k_a through a parameter $\gamma > 0$. When the contact condition is satisfied, i.e. two particles are less than a distance r_c apart, a linear axial spring with a stiffness of γk_a is placed between the contacting particles. Thus the potential energy associated with the contact between particles i and j is $U_{ij} = \frac{1}{2}\gamma k_\mathrm{a}(r_\mathrm{c} - r_{ij})^2$ when the particles are in contact (i.e. for $r_{ij} \le r_\mathrm{c}$), and $U_{ij} = 0$ when $r_{ij} > r_\mathrm{c}$. This simplified contact model is essential to the existence of multistable magneto-elastic configurations as it provides an equilibrium position when magnets are in attraction.

2.3. Dissipative interactions

Dissipation in the model is introduced in the form of viscous interactions. The value c_a is the damping coefficient associated with the rate of deformation of the axial springs. The damping associated with the rate of deformation of the contact interactions is βc_a, where $\beta > 0$ defines the damping coefficient during contact between particles relative to c_a. Thus the dissipative force between particles is $\boldsymbol{f}_{ij} = \beta c_\mathrm{a}\dot{r}_{ij}\boldsymbol{n}$ when $r_{ij} \le r_\mathrm{c}$, and $\boldsymbol{f}_{ij} = c_\mathrm{a}\dot{r}_{ij}\boldsymbol{n}$ for $r_{ij} > r_\mathrm{c}$. A similar definition is considered for dissipation associated with the deformation of the torsional springs, with c_τ defining the corresponding damping coefficient.

2.4. Energy functional and governing equations

The total energy stored by the lattice $\mathcal{E}_\mathrm{sys}$ is given by the sum of the kinetic energy T and the potential energy U:

$$\mathcal{E}_\mathrm{sys} = \sum_{n=1}^{N} T_n + U_n \tag{2}$$

where $n = 1, \ldots, N$ identifies all the particles in the lattice.

The set of governing equations describing the behavior of each particle and its interactions with connected units can be derived by the application of Lagrange's equations. The equation governing the motion of the i-th particle can be generally expressed as [4]:

$$\boldsymbol{M}_i\ddot{\boldsymbol{q}}_i + \sum_{j}^{J}\left[\boldsymbol{C}_j(\boldsymbol{q}_j)\dot{\boldsymbol{q}}_j + \boldsymbol{K}_j(\boldsymbol{q}_j)\boldsymbol{q}_j\right] = \boldsymbol{f}_i^{(m)}(\boldsymbol{q}_i, \ldots, \boldsymbol{q}_m, \ldots, \boldsymbol{q}_M) \tag{3}$$

where $\boldsymbol{q}_i \in \mathbb{R}^{3\times 1}$ is the vector of the generalized coordinates, while $\boldsymbol{M}_i, \boldsymbol{C}_j(\boldsymbol{q}_j), \boldsymbol{K}_j(\boldsymbol{q}_j) \in \mathbb{R}^{3\times 3}$ are mass, damping and equivalent stiffness matrices that describe inertial, dissipative and mechanical interactions of the particles with its J mechanically connected neighbors, while, $\boldsymbol{f}_i^{(m)} \in \mathbb{R}^{3\times 1}$ is the generalized force vector describing the magnetic interactions with the M magnetically connected particles.

3. Results

3.1. Analysis of equilibrium configurations

Because of magnetic interactions, the lattice can take different stable configurations, which correspond to different values of the angle θ (Fig. 2). When magnetized in the pattern shown (blue and red circles denote opposite magnetic polarizations),

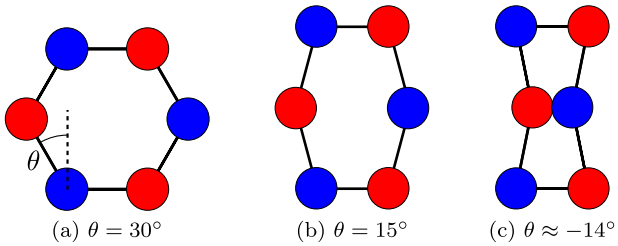

Fig. 2. (Color online.) Hexagonal (a) and re-entrant (c) lattices as two stable periodic equilibrium configurations. The angle θ describes the transition from one to the other and defines intermediate configurations (b). Red and blue circles denote magnets polarized into and out of the page respectively. Black lines represent elastic connections.

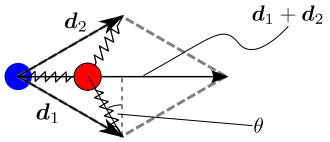

Fig. 3. (Color online.) Unit cell of the hexagonal lattice, lattice vectors, and main geometric parameters.

the hexagonal lattice (Fig. 2(a)) may reconfigure in stable configurations corresponding to various values of the internal angle θ, and may evolve into the re-entrant lattices of Fig. 2(c).

To understand which local configurations are possible, it is instructive to consider the unit cell of Fig. 3 as representative of an infinite, periodic lattice. This unit cell properly describes both regular hexagonal and re-entrant geometries as defined by the lattice vectors $\boldsymbol{d}_1$ and $\boldsymbol{d}_2$. The total energy for a unit cell $\mathcal{E}$ is given by the sum of the kinetic and potential energy:

$$\mathcal{E} = \sum_{e=1}^{E} T_e + U_e \tag{4}$$

where $e = 1, \ldots, E$ identifies the particles belonging to the unit cell. Local minima of this energy functional, restricted to the time constant terms, describe stable, periodic lattices [23]. These minima can be found through a Quasi-Newton optimization search algorithm [24]. The minimization problem at the unit cell level is formulated by considering as unknowns the generalized coordinates $\boldsymbol{q}$ of the particle inside the unit cell, i.e. the red particle in Fig. 3, and the lattice vectors $\boldsymbol{d}_1, \boldsymbol{d}_2$. The resulting optimization problem is thus expressed as:

$$\min_{\boldsymbol{u}} \quad \mathcal{E}(\boldsymbol{u}) \tag{5}$$

where $\boldsymbol{u} = [\boldsymbol{q}, \boldsymbol{d}_1, \boldsymbol{d}_2]$. The optimization procedure provides the geometry of the unit cell, which defines the internal angle θ, and the associated energy $\mathcal{E}$ for a given set of lattice parameters, i.e. k_a, k_τ, $\psi^{(m)}$, etc. Practically, this problem is solved by imposing the angle θ and then looking for the geometrical configuration associated with a stable equilibrium configuration. The solution of the nonlinear system of equations described by Eq. (5) is simplified by the following geometrical constraints: (1) the center red particle can only move along the horizontal center line of the unit cell which is defined by the vector resultant $\boldsymbol{d}_1 + \boldsymbol{d}_2$, and (2) the two lattice vectors are of equal magnitude, i.e. $d_1 = d_2$. These two constraints define θ and enforce the unit cell symmetry about its horizontal center line.

Equilibrium configurations are found for assigned values of $\theta \in [-20°, +35°]$ and for different magnetization levels. The loci of the corresponding equilibrium configurations are shown in Fig. 4 for three levels of magnetizations. The plots present the change in unit cell potential energy ΔU at equilibrium relative to the regular hexagonal unmagnetized case as a function of the imposed value of θ. In the plot of Fig. 4 and in the remainder of the paper, unit cell energy and magnetization parameter are respectively normalized as follows [4]:

$$\Delta\bar{\mathcal{E}} = \frac{2\Delta U}{k_a r_0^2} \tag{6}$$

where the denominator corresponds to the total energy stored by the axial spring when it is fully compressed and there is no contact (i.e. $r_{ij} = 0$, and $\gamma = 0$), with r_0 denoting the undeformed length of the axial springs, and

$$\bar{\psi}^{(m)} = \frac{\psi^{(m)}}{k_a r_0^5} = \frac{f^{(m)}(r_{ij} = r_0)}{k_a r_0} \tag{7}$$

which defines the ratio of the magnetic force at $r_{ij} = r_0$ to the force required to fully compress the axial spring in the absence of contact, i.e. $k_a r_0$. Hence, $\bar{\psi}^{(m)}$ provides a comparison of the strength of the magnetic interactions relative the axial spring restoring force.

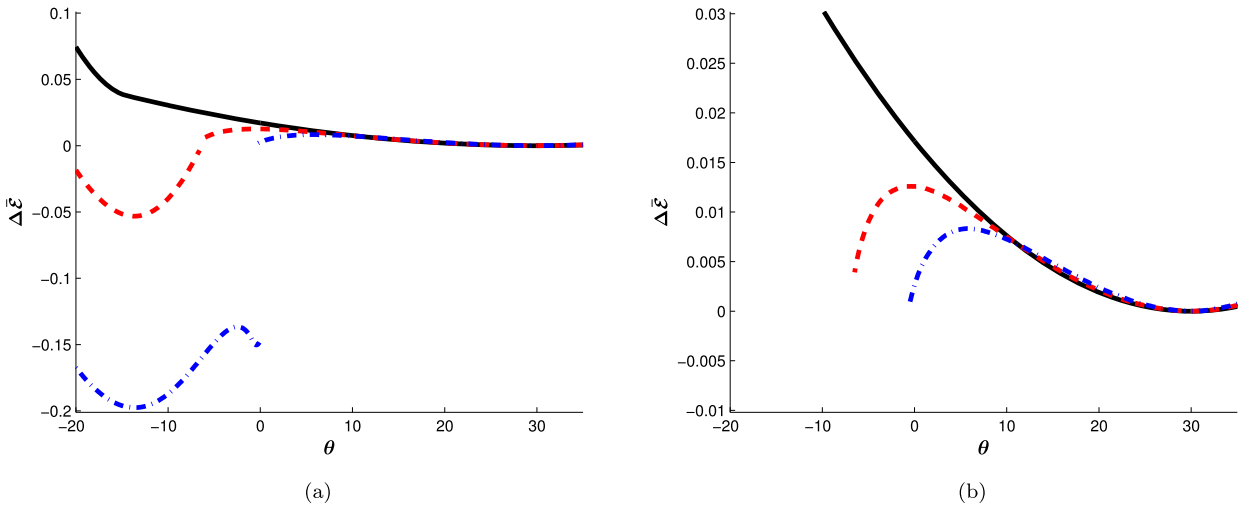

Fig. 4. (Color online.) Equilibrium loci for the unit cell as a function of internal angle θ: $\bar{\psi}^{(m)} = 0$ (black $-$), $\bar{\psi}^{(m)} = 0.02$ (red $--$), and $\bar{\psi}^{(m)} = 0.05$ (blue $-\cdot-$) (a), and $10\times$ zoom for detailed view in the $\theta > 0$ range (b).

The magnetization levels considered in Fig. 4 are $\bar{\psi}^{(m)} = 0, 0.02, 0.05$, while the lattice is defined by the following parameters: $\gamma = 39$, $r_c = 0.5$, $c_a/m = 0.4\ \text{s}^{-1}$, $c_\tau/(mr_0^2) = 0\ \text{s}^{-1}$, $\beta = 50$, $I/(mr_0^2) = 1/32$, $\omega_0 = \sqrt{k_a/m} = 1$ rad/s, $\omega_r = \sqrt{k_\tau/I} = \sqrt{1/2}$ rad/s. In Fig. 4, the curve corresponding to the unmagnetized case, ($\bar{\psi}^{(m)} = 0$) is continuous, with a noticeable slope discontinuity near $\theta = -15°$ which corresponds to the initial contact between particles. Of note is the fact that the initial, regular hexagonal case $\theta = 30°$ is the most energetically favorable configuration, which therefore indicates that a lattice perturbed from this initial configuration is likely to return to it without undergoing any reconfiguration. The energetic advantage of this initial configuration is clearly shown in the detailed plot of Fig. 4(b). Thus, configurations with re-entrant angle and contact would require additional energy to be provided for the system to evolve into them from an initial configuration of $\theta = 30°$. The magnetized cases, in contrast, have a significantly different behavior as indicated by the discontinuous red and blue dashed lines in Fig. 4. The range for $\theta > 0$ looks essentially identical to the case for $\bar{\psi}^{(m)} = 0$, while re-entrant magnetized configurations are characterized by equilibrium topologies associated with significantly lower energy levels. This indicates that the magnetized lattices, if provided enough energy in the form of external perturbations, can indeed evolve and transition to a different stable equilibrium topologies with $\theta < 0$. The amounts of energy that enable such a transition cannot be directly estimated from the curves in Fig. 4 as the dynamic terms associated with inertias and dissipation need to be accounted for in order to evaluate the transition through a saddle point in the energy profile, which is here not shown and not directly estimated. As expected, the energetic levels of the re-entrant equilibrium configurations for the magnetized lattices are lower for increasing magnetization levels. This is consistent with the fact that the magnets are all arranged in attraction due to their alternate polarization distributions. One may consider cases where repulsive configurations are present, which would lead to different topologies and periodic lay-outs defined by the distributions of magnetic polarizations.

The next section illustrates how these investigations can aid the interpretation of the dynamic behavior of the considered class of lattices and potentially inform their design for multi-stability.

3.2. Dynamic reconfiguration

To gather information about how lattice magnetization can affect the transformation of the 2D magneto-elastic lattice, numerical simulations are performed by integrating the equations of motion (Eq. (3)) in time. A finite lattice is considered with a number of cells chosen so that boundary effects can have minimum influence on the transient behavior of the central portion of the lattice. The initial configuration for the finite lattice is determined by imposing an initial angle $\theta = 30°$ and determining the lattice vectors as a function of the applied magnetization levels, and assuming that all springs are at rest when the lattice is in the initial regular hexagonal configuration in the absence of magnetization. Solution of the equilibrium configurations through minimization of the energy function for the entire finite lattice defines the initial geometry. Such geometry may be slightly different in the presence of magnetization, due to the magnetic attraction that leads to small changes in the lattice vectors. Such changes, which are accounted for in the simulations, are however too small to be noticeable from the graphical representation of the lattice, given the small magnetization levels considered and the forces that are only a few percent of the magnitude of the spring restoring forces. Once the initial equilibrium configuration is identified, boundary conditions are applied to enforce the stability of the lattice and to avoid rigid body motions. The choice of the equilibrium conditions are based on the choice of enforcing symmetry along the mid horizontal line under an equally symmetric load distribution, which in this case is a horizontal point force applied at the middle point of the left vertical

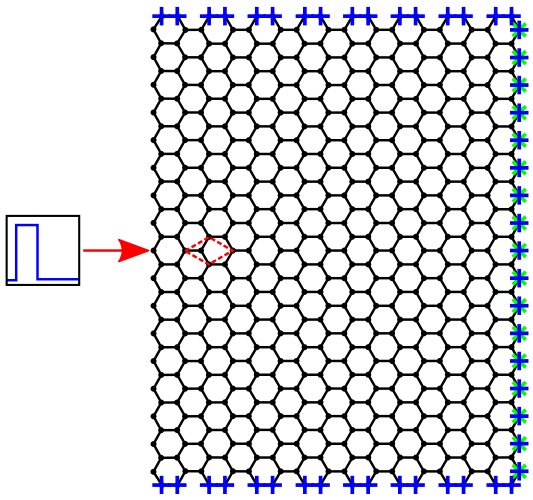

Fig. 5. (Color online.) Numerical simulation setup for finite lattice. Black lines represent axial springs and black dots represent magnetized masses. Green "×"s denote constraint of horizontal displacements, and blue "+"s denote constraint of vertical motion. The dashed red lines show a unit cell for which energy is plotted in Fig. 7.

boundary. The selected boundary conditions are pins constraining horizontal and vertical displacements along the vertical right boundary, and roller-type constraints along the top and bottom edges to constrain only the vertical displacements. Along all boundaries, rotations remain unconstrained. A schematic of the finite lattice with point of loading and boundary conditions is shown in Fig. 5.

All simulations are conducted by applying a force varying in time as a rectangular pulse at the location shown. Pulse duration and amplitude are chosen empirically to be sufficient to induce transition in the magnetized cases. The energy associated with the pulse is sufficient to compensate for the energy needed to transition from the initial stable configuration to another in the case of multi-stable layouts. Such energy must overcome all kinetic contributions and dissipation terms. All simulations consider a pulse width of 0.08π s and an amplitude $F_0 = 6k_a r_0$. The response of the three different structures is presented in Fig. 6. In the unmagnetized case, this pulse perturbs the lattice, but it does not cause its re-configuration, since upon removal of the force the lattice returns to its initial configuration, which is the most energetically favorable. As a result no transition occurs in the lattice, as shown in Fig. 6(c). For $\bar{\psi}^{(m)} = 0.02$ the system becomes multistable. The re-entrant configuration has a lower energy. Therefore, energy will be released into the lattice during the transformation, with the potential to aid in further reconfiguration. Given the 2D geometry of the lattice, the energy associated with the input force decays with the distance from the point of application due to geometrical spreading. This leads to the re-configuration to be only observed over a limited region of the lattice, within which the cells receive sufficient energy to transition to the lower energy states corresponding to the re-entrant configuration (Fig. 6(d–f)). For a higher magnetization, i.e. $\bar{\psi}^{(m)} = 0.05$, the entire lattice reconfigures by the end of the simulations due to the lower energetic level observed at the unit cell level for this magnetization (Fig. 6(g–h). The study of the dynamic behavior of the lattice can also be observed in terms of the energy within a unit cell. Specifically, the cell highlighted by the red dashed line in Fig. 5 is observed at various instants of time during the simulations. These variations are overlaid on the equilibrium curves for the corresponding magnetization levels in Fig. 7. The resulting plots show the time evolution of the trajectory of the unit cell configuration and its energy as black dots, while the minimum energy curve is the solid red curve. Each black dot shows the energy at an instant, evenly spaced in time, and the red curves are the curves of Fig. 4 without the shift. The plots illustrate how such configurations evolve dynamically from the initial configuration to a final. All the simulations begin at the local minimum at $\theta = 30^\circ$, which is the hexagonal lattice configuration. Then the cell energy increases due to the applied force, and through the dynamics of the structure it oscillates about and progresses to its final local energy minimum. Such oscillations are shown in the inset of the figures for better clarity. Note that all energy trajectory points are above the red curve for all intermediate dynamic configurations, which illustrates how the curve correctly provides a lower bound for the energy content of the unit cell under consideration. In the absence of magnetization (Fig. 7(a)) the unit cell undergoes significant distortions due to the forcing as illustrated by the large variations of the internal angle θ, which temporarily reaches negative values, but it returns to oscillate around the initial configuration. This is because there is no other equilibrium position for it to stop at. The magnetized cases shown in Fig. 7(b, c) clearly illustrate the transition of the unit cell energy from the initial configuration at $\theta = 30^\circ$ to the re-entrant state near $\theta = -15^\circ$, which is the point of arrival upon removal of the force and the free motion of the lattice.

Returning to Fig. 6, it is worth noting that the pattern of reconfiguration is not uniform and appears to be characterized by a pattern which is common to both magnetization cases. The results seem to suggest the existence of a triangular transition front that does not propagate uniformly within the lattice. The pattern of propagation of this front may be affected by the underlying isotropy, or lack thereof, of the lattice, which in turn is determined by the unit cell geometry.

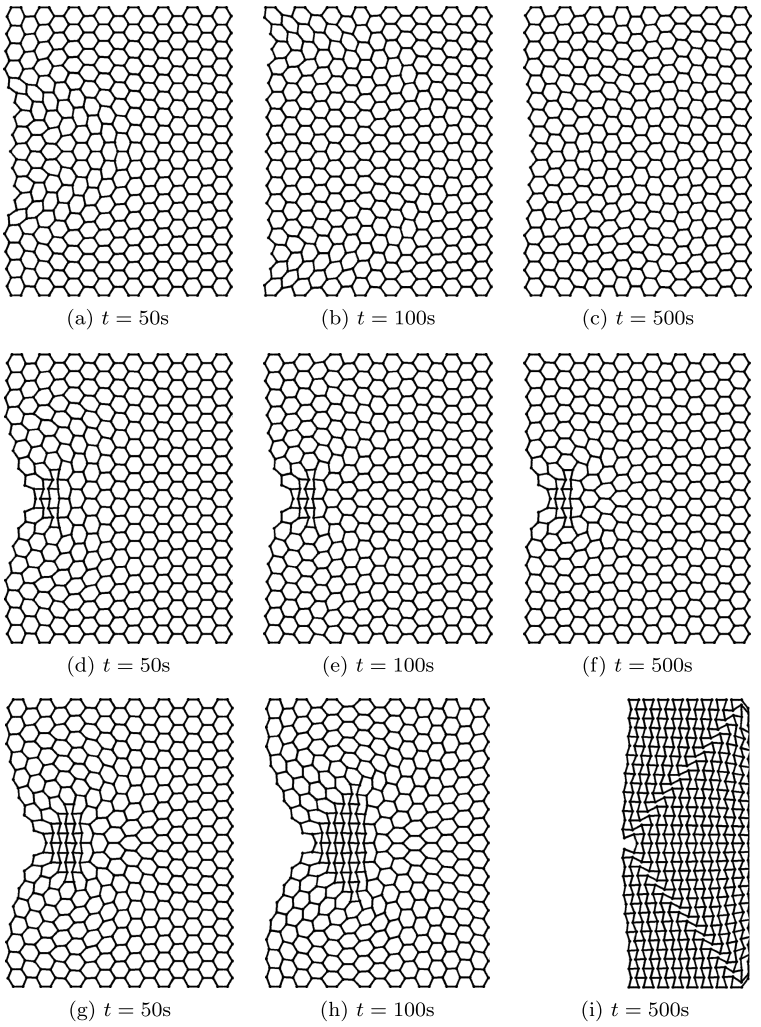

Fig. 6. Snapshots of deformed configuration of the lattices observed during dynamic simulations: $\bar{\psi}^{(m)} = 0$ (a–c), $\bar{\psi}^{(m)} = 0.02$ (d–f), and $\bar{\psi}^{(m)} = 0.05$ (g–i).

This aspect certainly deserves further investigation as it may have significant implications for the design of multi-stable lattices with desirable transition front propagation characteristics. Of note is also the fact that the energy profile of the $\bar{\psi}^{(m)} = 0.05$ structure allows faster reconfiguration for the same forcing, which is observed in comparing Fig. 6(d–e) and Fig. 6(g–h). This is likely because more energy is available to be converted into kinetic energy. The final configuration of the $\bar{\psi}^{(m)} = 0.05$ case (Fig. 6(i)) is much different than the initial configuration and the final configuration of the $\bar{\psi}^{(m)} = 0.02$ case. It has a much higher density and is composed entirely of anisotropic cells. Three sub-regions of re-entrant cells are separated by two bands of cells oriented approximately perpendicularly to the others. These bands can be denoted as "transition bands" [4]. The transition bands are the result of the dynamic reconfiguration of the lattice, and different forcing has been observed to produce different numbers and positions of transition bands. The local geometric variations seen in the transition bands affect the propagation of waves and are expected to aid in wave steering and energy absorption.

Finally, in simulating the collapse of magneto-elastic lattices such as those presented here it is observed that the damping characteristics of the system can greatly affect the dynamics of the system, which can ultimately change the final configuration. For the aforementioned study, the damping was all kept constant for simplicity, but if structures such as these are to be dynamically reconfigured in a predictable way, the effect of damping must be taken into account and properly characterized. For example, increasing the contact damping parameter β helps prevent overshooting when particles come into contact near their secondary stable position. To illustrate this, β is reduced to 5 from 50 for the $\bar{\psi}^{(m)} = 0.02$ case and the simulation is repeated. Shown in Fig. 8(a–c), it is clear that the change in β does not allow some of the particle pairs to remain in contact. Instead, they bounce out of the local energy minimum and the final configuration has only one collapsed cell. It has also been observed that increasing the torsional damping c_τ allows the system to better distribute the applied force transversely, similar to increasing the viscosity of a fluid. For reference, in Fig. 6 there is no torsional damping. To contrast this, simulations of the $\bar{\psi}^{(m)} = 0.02$ case

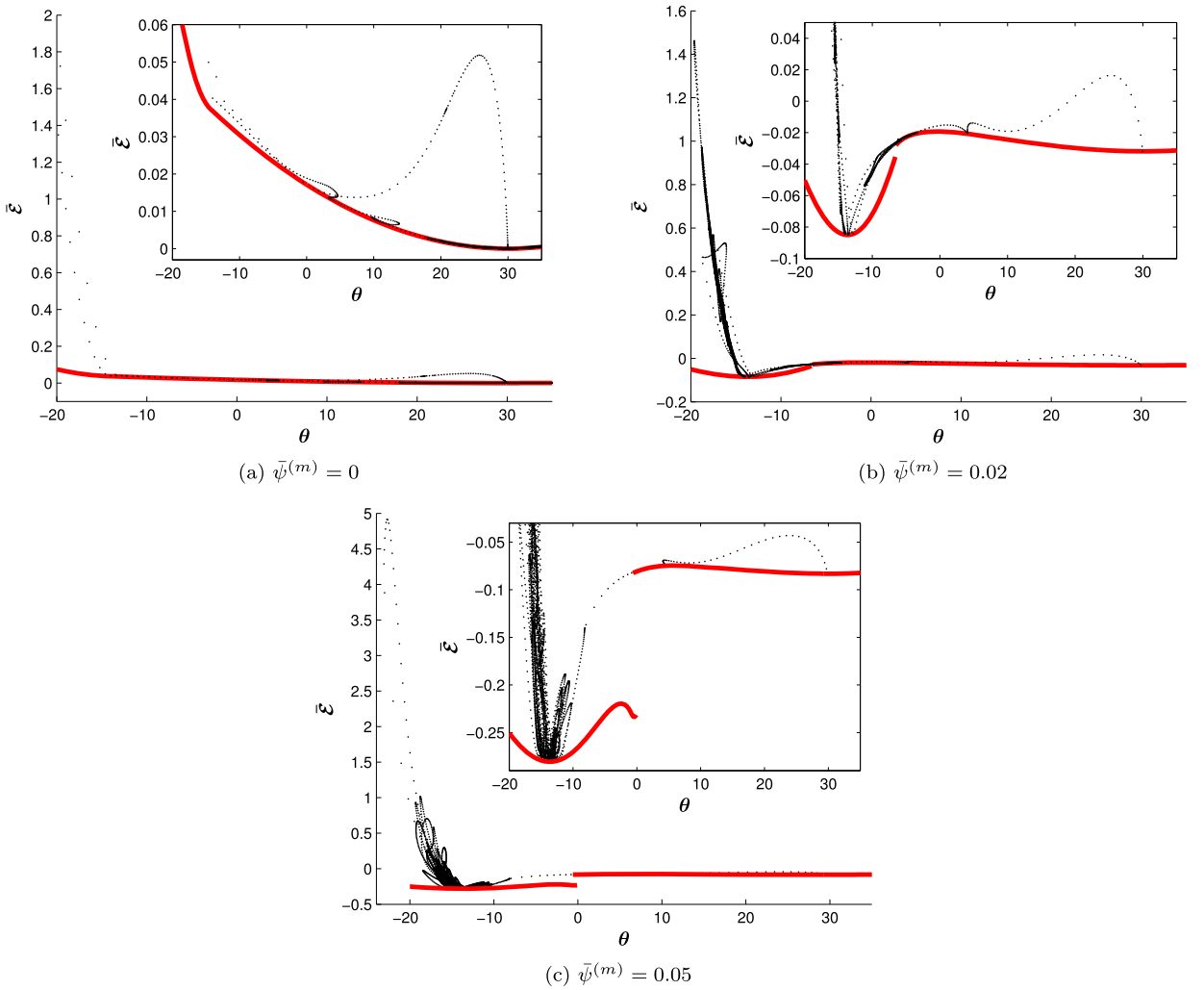

(a) $\bar{\psi}^{(m)} = 0$ (b) $\bar{\psi}^{(m)} = 0.02$

(c) $\bar{\psi}^{(m)} = 0.05$

Fig. 7. (Color online.) Normalized potential energy $\bar{\mathcal{E}}$ of the unit cell highlighted in Fig. 5 for the three simulations discussed shown as the cell exhibits different values of θ during deformation.

with $c_\tau/(mr_0^2) = 0.05$ s^{-1} and 0.50 s^{-1} were run. The first case (Fig. 8(d–f)) shows deformation spread more evenly across the left side of the structure than in Fig. 6(d–f) and results in only 3 collapsed cells in response to the forcing instead of 6. The second case (Fig. 8(g–i)) shows that with sufficient torsional damping the applied force will be distributed and dissipated so well that no reconfiguration can occur under the applied load. These 3 examples are merely an example of how reconfiguration can be further tailored through damping, and this aspect requires further investigation.

4. Conclusion

The dynamic reconfiguration of 2D multistable magneto-elastic structures is shown to be dependent on the magnetization of the lattice. Varying magnetization while keeping forcing constant can control whether or not reconfiguration occurs, the rate at which a structure reconfigures, and the final configuration. This dependence is the result of magnetization affecting the minimum energy required to transition and the energy released due to the hexagonal to re-entrant reconfiguration. Geometrical spreading and lattice isotropy also determine the shape of a transition front, which seems to occur according to repeatable pattern. This and the prediction of the final configuration of the structure is of greatest interest to the authors due to the implications it has for producing structures that can adapt their functions and properties through reconfiguration. The information presented here provides insight into the ways in which 2D magneto-elastic structural reconfiguration can be controlled. This study motivates future investigations on the analysis of transition paths and final configurations that will aid the design of reconfigurable architectured materials and devices.

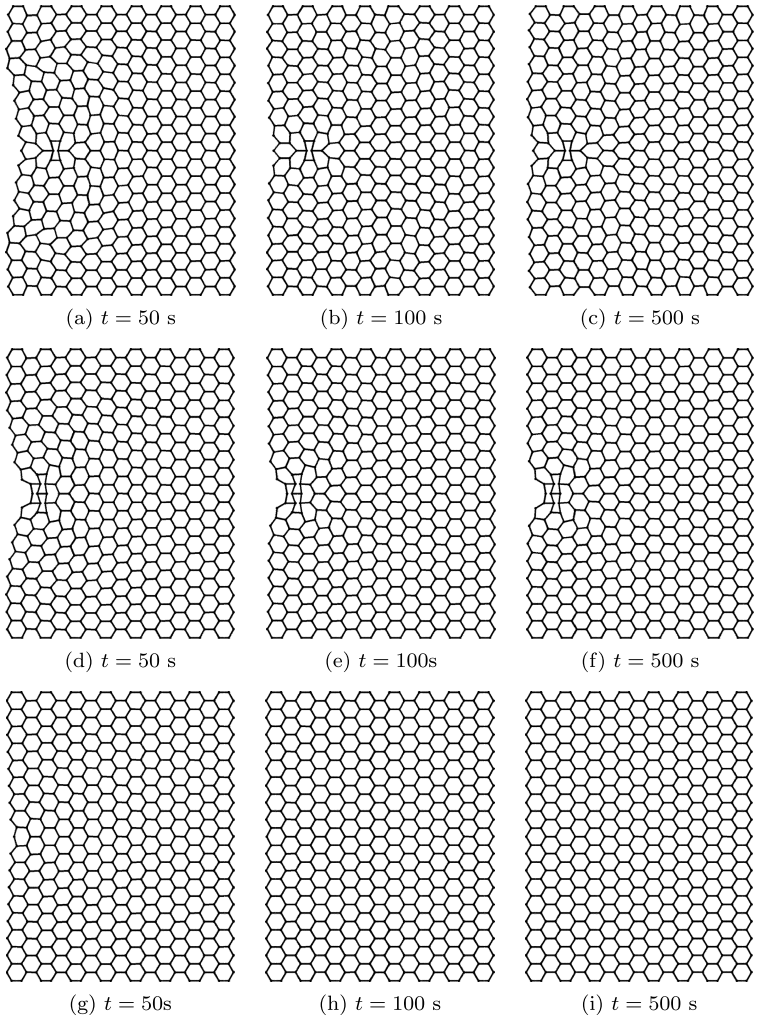

Fig. 8. Snapshots of the lattices with $\bar{\psi}^{(m)} = 0.02$ observed during dynamic simulations with different damping parameters: $\beta = 5$ (a–c), $c_\tau/(mr_0^2) = 0.05$ s^{-1} (d–f), and $c_\tau/(mr_0^2) = 0.50$ s^{-1} (g–i). Other lattice parameters are left unchanged.

Acknowledgements

This research was funded by a grant from the Air Force Office of Scientific Research (AFOSR) grant number FA9550-13-1-0122, monitored by Dr. David Stargel, whose input and guidance are acknowledged and appreciated. The work of Shane Lympany, who had a significant part in building the computational tools used in this research, is also acknowledged and appreciated.

References

[1] L.J. Gibson, M.F. Ashby, Cellular Solids: Structure and Properties, Cambridge University Press, Cambridge, UK, 1999.
[2] S. Gonella, M. Ruzzene, Analysis of in-plane wave propagation in hexagonal and re-entrant lattices, J. Sound Vib. 312 (1) (2008) 125–139.
[3] F. Casadei, J.J. Rimoli, Anisotropy-induced broadband stress wave steering in periodic lattices, Int. J. Solids Struct. 50 (9) (2013) 1402–1414.
[4] M. Schaeffer, M. Ruzzene, Wave propagation in multistable magneto-elastic lattices, Int. J. Solids Struct. 56–57 (2015) 78–95.
[5] J.O. Vasseur, O. Bou Matar, J.-F. Robillard, A.-C. Hladky-Hennion, P.A. Deymier, Band structures tunability of bulk 2D phononic crystals made of magneto-elastic materials, AIP Adv. 1 (4) (2011) 041904.
[6] Joseph N. Grima, Roberto Caruana-Gauci, Mirosław R. Dudek, Krzysztof W. Wojciechowski, Ruben Gatt, Smart metamaterials with tunable auxetic and other properties, Smart Mater. Struct. 22 (8) (2013) 084016.
[7] Joseph N. Grima, Elaine Chetcuti, Elaine Manicaro, Daphne Attard, Matthew Camilleri, Ruben Gatt, Kenneth E. Evans, On the auxetic properties of generic rotating rigid triangles, Proc. R. Soc. A, Math. Phys. Eng. Sci. 468 (2139) (2012) 810–830.
[8] K. Bertoldi, M.C. Boyce, Mechanically triggered transformations of phononic band gaps in periodic elastomeric structures, Phys. Rev. B 77 (5) (2008) 052105.
[9] Katia Bertoldi, Pedro M. Reis, Stephen Willshaw, Tom Mullin, Negative Poisson's ratio behavior induced by an elastic instability, Adv. Mater. 22 (3) (2010) 361–366.

[10] P. Wang, F. Casadei, S. Shan, J.C. Weaver, Katia Bertoldi, Harnessing buckling to design tunable locally resonant acoustic metamaterials, Phys. Rev. Lett. 113 (1) (2014) 014301.
[11] Katia Bertoldi, Sung Hoon Kang, Sicong Shan, Francisco Candido, Shape programmable structures, in: ASME 2014 International Mechanical Engineering Congress and Exposition, IMECE2014, 2014.
[12] V.V. Smirnov, O.V. Gendelman, L.I. Manevitch, Front propagation in a bistable system: how the energy is released, Phys. Rev. E 89 (5) (2014) 050901.
[13] N. Nadkarni, C. Daraio, D.M. Kochmann, Dynamics of periodic mechanical structures containing bistable elastic elements: from elastic to solitary wave propagation, Phys. Rev. E 90 (2) (2014) 023204.
[14] A. Cherkaev, E. Cherkaev, L. Slepyan, Transition waves in bistable structures, I delocalization of damage, J. Mech. Phys. Solids 53 (2) (2005) 383–405.
[15] L. Slepyan, A. Cherkaev, E. Cherkaev, Transition waves in bistable structures, II: analytical solution: wave speed and energy dissipation, J. Mech. Phys. Solids 53 (2) (2005) 407–436.
[16] L.I. Slepyan, M.V. Ayzenberg-Stepanenko, Localized transition waves in bistable-bond lattices, J. Mech. Phys. Solids 52 (7) (2004) 1447–1479.
[17] Venkata Suresh Guthikonda, Ryan S. Elliott, Modeling martensitic phase transformations in shape memory alloys with the self-consistent lattice dynamics approach, J. Mech. Phys. Solids 61 (4) (2013) 1010–1026.
[18] L. Truskinovsky, Anna Vainchtein, Kinetics of martensitic phase transitions: lattice model, SIAM J. Appl. Math. 66 (2) (2005) 533–553.
[19] Felix E. Hildebrand, Rohan Abeyaratne, An atomistic investigation of the kinetics of detwinning, J. Mech. Phys. Solids 56 (4) (2008) 1296–1319.
[20] O. Kastner, G.J. Ackland, Mesoscale kinetics produces martensitic microstructure, J. Mech. Phys. Solids 57 (1) (2009) 109–121, cited by [17].
[21] É. du Trémolet de Lacheisserie, D. Gignoux, M. Schlenker (Eds.), Magnetism: Fundamentals, Springer, 2005.
[22] K.W. Yung, P.B. Landecker, D.D. Villani, An analytic solution for the force between two magnetic dipoles, Magn. Electr. Sep. 9 (1998) 39–52.
[23] H. Goldstein, Classical Mechanics, Addison–Wesley Publishing Company, Inc., 1953.
[24] S.S. Rao, Engineering Optimization: Theory and Practice, 4th edition, John Wiley & Sons, 2009.